J Opt (February 2024) 53(1):342–353
https://doi.org/10.1007/s12596-023-01230-w

RESEARCH ARTICLE

Design and analysis of performance parameters for achieving high efficient ITO/PEDOT:PSS/P3HT:PCBM/Al organic solar cell

Chandra Shekhar Kundu[1] · Apurba Adhikary[1,2] · Md. Shamim Ahsan[1] · Abidur Rahaman[2] · Md. Bipul Hossain[2] · Avi Deb Raha[3] · Saydul Akbar Murad[4] · Farid Ahmed[5]

Received: 4 January 2023 / Accepted: 16 May 2023 / Published online: 1 June 2023

Abstract In this study, we designed a highly efficient ITO/PEDOT:PSS/P3HT:PCBM/Al-based bulk heterojunction organic solar cell. We investigated the performance of various optical and electrical properties of the designed organic solar cells. We improved the power conversion efficiency by using appropriate materials in different layers of the organic solar cells and refractive index and lattice constant matching among the layers. GPVDM simulator was used for simulating various properties of the organic solar cells, such as current density, voltage density, fill factor, and power conversion efficiency. Various parameters of the active layer of the organic solar cells were varied for optimization. In addition, we analyzed the impact of the thickness of the active layer and device series resistance on the improvement of the power conversion efficiency of the organic solar cells. Maximum power conversion efficiency of 16.46% with a fill factor of 74.09% was obtained for a series resistance of 15 ohms. We observed an inversely proportional relationship between power conversion efficiency and series resistance. We optimized the value of the thickness of the active layer as 75 nm while designing the organic solar cells to achieve maximum power conversion efficiency. We strongly believe that the proposed organic solar cell model will play a significant role in achieving high PCE organic solar cells.

Keywords Organic solar cell (OSC) · Power conversion efficiency (PCE) · Fill factor (FF) · Performance parameters · Series resistance · Thickness

✉ Apurba Adhikary
apurba@nstu.edu.bd

✉ Md. Shamim Ahsan
shamim@ece.ku.ac.bd

[1] Electronics and Communication Engineering (ECE) Discipline, Science Engineering and Technology (SET) School, Khulna University, Sher-E-Bangla Road, Khulna 9208, Bangladesh

[2] Department of Information and Communication Engineering (ICE), Noakhali Science and Technology University, Noakhali 3814, Bangladesh

[3] Computer Science and Engineering (CSE) Discipline, Science Engineering and Technology (SET) School, Khulna University, Sher-E-Bangla Road, Khulna 9208, Bangladesh

[4] Faculty of Computing, College of Computing and Applied Sciences, Universiti Malaysia Pahang, Kuantan, Malaysia

[5] Manufacturing and Industrial Engineering, University of Texas Rio Grande Valley, 1201 W University, Edinburg, TX 78539, USA

Introduction

Dwindling reserves of conventional energy sources such as crude oil and coal have been a foremost source of international clash in the past few epochs. In addition, extensive pollution and consequent climate change is the conspicuous cause of the deterioration of human health and damage to infrastructure in numerous countries. Moreover, the latest disaster in Japan has encouraged many countries to phase out nuclear power, which was caused owing to leakage in nuclear power plants. A large variety of disasters increased the importance of renewable energy sources such as wind, solar, hydropower, and bio-thermal. The International Energy Agency stated that renewable energy sources are expected to be considered as the second largest power source to overtake natural gas in the near future [1]. A huge amount of energy, i.e., 1.75×1017 J, is required for the earth to be given by the sun to draw attention while searching for an alternative source of energy. In fact, not more than 1 h is required to fulfill this demand if we consider a total energy usage of 4.4×1020 J (as in 2003) per year. However, tying

together this energy in a simple and cost-effective way is not easy to handle and execute. A bunch of technologies are required to be employed. The first step is the conversion of sunlight into thermal energy, which can consequently be used for heating, hot water or transformation into electrical energy. Instead, the photovoltaic effect can directly convert sunlight into electrical energy. Currently, inorganic silicon-based solar cells are dominating in the field of photovoltaics [2]. Solar radioactivity is a tremendously underutilized source of energy that needs to be converted into electricity. Photovoltaics-based inorganic materials such as germaniums and silicon have the capability to advance in trapping this source of energy by means of direct conversion of radiation to electricity. Nevertheless, organic solar cells have been becoming popular in the modern era, and it is expected that their bloom is approaching. OSCs have become popular and attractive topics because of the inconvenient production process and material shortage of inorganic solar cells. OSC uses small organic molecules or conductive organic polymers for light absorption and charge transport. Proper materials selection has made OSCs as a potential lucrative candidate for photovoltaic applications with flexible organic molecules. Organic solar cell provides several advantages compared to the inorganic solar cell. The OSC provides services with lower cost, easy processing ability, potentially unbreakable or flexibility, and adequately large and friendly environment [3–6]. In addition, OSCs have been applied in a lot of sectors, including residential home systems or commercial building systems, water pumping, telecommunication, automobiles, space power supply, photovoltaic power plants, public system power supply, military, and other digital consumption [3, 5]. However, OSCs have not still achieved commercial success of photovoltaic devices due to the low-power conversion efficiency and durability of OSCs. In this paper, we examined the performance of various parameters to improve the power conversion efficiency. Our computational investigation focused on the use of materials' properties and thickness improvement as a means of enhancing OSC performance. Specifically, we explored the use of different morphological features, such as the thickness and distribution of the active layer, to optimize device performance. The computational approach has the benefit of efficient and equivalent questioning of large number of materials' properties and thickness by apprehending the physics of charge generation and transportation in OSCs. We developed an efficient and scalable framework for simulation of OSC devices that is dimensionally independent although OSC simulation models for heterogeneous structures have been considered previously [7–11].

Although, three types of OSCs are available at present (single layer, bilayer, and bulk heterojunction), bulk heterojunction photovoltaic organic solar cells are the most popular and energy-efficient OSC. In bulk heterojunction organic solar cell (BHJOSC), a polymer blend made by a mixture of electron donor and acceptor together is sandwiched between the electrodes. If the polymers blend length is equal to the exciton diffusion length, maximum number of the generated excitons can reach the interface and can be separated efficiently to the opposite electrodes [12]. BHJOSC based on conjugated polymers blends and fullerene acceptors become important because of its potentiality to convert sunlight into electricity [13–16]. Power conversion efficiency (PCE) can be improved significantly by combining proper choice of materials during designing, donor and acceptor phases for self-assembly, control of interface, and changing parameters in active layer [15]. Higher optical and electrical absorption is required for improving PCE in organic solar cells which can be controlled by light trapping techniques. Light trapping techniques in ray optics had been used for the improvement of optical and electrical absorption: micro-prism structure [17], collector mirrors [16], and V-folded configurations [18]. Niggemann et al. applied micro-prism structure for the trapping of light and improvement of absorption in the active layer. In this research, the thickness of the PEDOT and active layer was 100 nm but covering of polymer layers was not constant. As a result, the fill factor and a PCE (1%) was lower as compared to the flat cells (PCE: 4%) [17]. Liu [19] achieved 5.4% and 7.0% PCE by using P3HT and the derivatives of C60. Both Heliatek of Germany and Konarka Technologies of US manufactured the OSCs with 8.3% PCE [20, 21]. The Mitsubishi Chemical organization of Japan reported a PCE of 9.26% [22]. A group of researchers of AIST and PVTEC reported a PCE of 13.6% [23]. A. Kowsar et al. [24] reported a comparative analysis on solar cell simulators where they discussed about major thirteen simulators including Gpvdm, AFORS-HET, PC1D, AMPS-1D, and declared Gpvdm as the best simulator for designing organic solar cells. Another research group reported a review on solar cell fundamentals and technologies and predicted an increase of PCE above 15% in near future [25]. Another research group reported a survey on solar cell materials and a PCE of 12% for organic solar cell and projected a PCE above 15% in future [26]. R. Rabeya and F. Hakim reported a new design to improve the PCE of the organic solar cell up to 14.69% PCE and 78.13% fill factor [27]. Singh et al. [28] proposed a PCE of 12.87% which was achieved by optimizing the physical parameters of the plastic PTB7:PC71BM-based bulk heterojunction organic solar cell. Ogata et al. proposed a PCE of 0.58% which was achieved practically by increasing short-circuit current, achieved by adding electrodes to the CNT composite paper in the grid patterns [29]. Meredith and Armin proposed next-generation solution for organic and perovskite solar cells and addressed the difficulties and challenges for the solution in processing photovoltaic technologies [30]. Zhou et al. [31] achieved a PCE of 14.34% for organic solar cell by optimizing hierarchical

materials' properties and thickness in the bulk heterojunction active layer. Still there is scope of increasing the power conversion efficiency of organic solar cells.

In this study, we analyzed the performance of the designed OSCs based on the overall efficiency and improved the power conversion efficiency of OSCs. Firstly, we designed a highly efficient ITO/PEDOT:PSS/P3HT:PCBM/Al-based bulk heterojunction organic solar cell. We investigated various properties of the materials of different layers, i.e., light absorption, refractive index matching, and electrical and optical properties. In addition, we improved the PCE of organic solar cells by altering the materials of different layers of the OSCs and matching the refractive indices among the layers. We studied the electrical, optical, and other properties of different materials to increase photon to electron conversion for improved PCE. We used GPVDM (OPVDM) simulator to simulate our OSC's design and analyzed various properties including current density, voltage density, fill factor, and power conversion efficiency. Furthermore, the impact of variation of various active layer parameters, i.e., thickness and series resistance on the power, current density, and voltage of the OSC, is analyzed for improving the PCE. We achieved maximum power conversion efficiency of 16.46% with fill factor of 74.09% at a series resistance of 15 Ω. The proposed models of organic solar cells have potentials for commercialization.

Materials and methods

The primary objective of this paper is to design and simulate a high efficiency organic solar cell. We designed and simulated our proposed using GPVDM simulator and analyzed the performance of different parameters to achieve highly efficient organic solar cells.

Material properties

Our proposed bulk heterojunction organic solar cell consists of four layers: anode, organic-based electrode, active layer, and cathode. We selected ITO (indium tin oxide) on a glass substrate as the anode (electrode) because of its high transparency, i.e., transparent conductive oxide which enhanced the photosensitive properties of the cell. In our design, we used poly(3, 4-ethylene dioxythiophene):poly(styrenesulfonate) (PEDOT:PSS) as the organic-based electrode (hole transporting layer) which is used to assist charge extraction and injection providing a superior matching with the higher occupied molecular orbital (HOMO) energy level of donor [13, 32–34]. We selected P3HT:PCBM as an active layer which is a combination of donor (P3HT) and acceptor (PCBM). The donor (P3HT)—acceptor (PCBM) concentration of P3HT:PCBM controls the solar cell performance by means of power conversion efficiency. To account for the presence of two different materials in a heterojunction form, we used a multi-scale approach. At the atomistic level, we modeled the interaction between P3HT and PCBM using a force field. We then used this information to parameterize a coarse-grained model of the blend. The coarse-grained model allowed us to simulate the materials' properties and thickness of the blend on a larger length scale and over longer time scales, which enabled us to investigate the impact of materials' properties and thickness on the performance of OSCs. In addition, we used aluminum (Al) as a cathode because of its stability and higher electrical conductivity [25, 26]. For our design and simulation, we selected the materials for the four layers of OSC and considered various materials' properties, i.e., refractive index, lattice constant, and thickness. We analyzed the performance of various parameters of active layer and varied the thickness of the active layer to optimize the best design along with the highest power conversion efficiency of organic solar cell. Table 1 summarizes the physical parameters of the different layers of our designed organic solar cell (OSC).

Design parameters of the proposed OSCs

We start our research with a basic design of a bulk heterojunction solar cell of ITO/PEDOT:PSS/P3HT:PCBM/Al, basic device diagram of which is illustrated in Fig. 1. After we accomplished the basic design, we changed different parameters of active layer and thickness of the active layer to increase the power conversion efficiency of the OSC. In our design of OSCs, we fixed the thickness of different layers except active layer, i.e., P3HT:PCBM layer. The parameters that correspond to the materials' properties and thickness of the blend in our simulation software are the spatial distribution of P3HT and PCBM molecules and their orientation.

Table 1 Physical parameters of different layers of the OSCs [35]

Layer name	Thickness (nm)	Refractive index	Lattice constant (Å)	Material
Anode	150	1.86 @ 650 nm	$a=4.914$ $b=5.405$	ITO
Organic-based electrode	50	1.49 @ 658 nm	–	PEDOT:PSS
Active layer	Varied	1.98 @ 649 nm	–	P3HT:PCBM
Cathode	100	1.56 @ 650 nm	4.046	Al

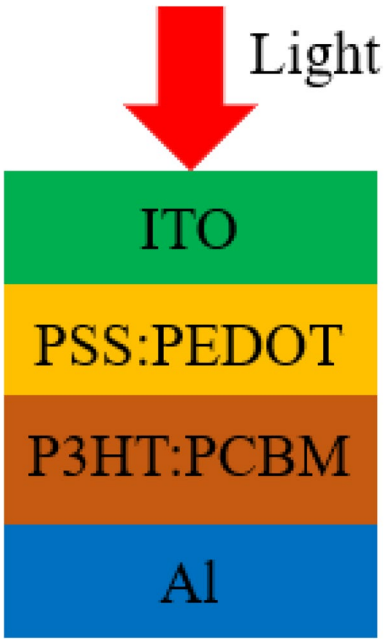

Fig. 1 Basic device structure of bulk heterojunction solar cell

We used these parameters to calculate the electron and hole density in the active layer, as well as other important parameters such as open-circuit voltage, short-circuit current, fill factor, maximum power output, and power conversion efficiency.

We investigated open-circuit voltage, short-circuit current, fill factor, maximum power output, and power conversion efficiency of the designed OSCs for different parameters of active layer such as electron mobility, hole mobility, effective density of free electron states, effective density of free hole states, electron trap density, and hole trap density. The default parameters of density of states of the active layer, i.e., P3HT:PCBM, are summarized in Table 2.

Model of OSC

Figure 2 demonstrates the GPVDM software window for various settings of the proposed solar cell structure. The opening window of GPVDM software is demonstrated in Fig. 2a. Afterward, we selected different types of materials for different layers of organic solar cell. The GPVDM window of device structure after modeling organic solar cell is depicted in Fig. 2b. We changed the materials of different layers and their thickness for optimizing power conversion efficiency of the OSCs. Figure 2c illustrates the GPVDM window to vary different parameters of various layers of the OSCs for comparison.

Results and discussion

The most essential optical and electrical parameters of the organic solar cells such as open-circuit voltage (V_{OC}), short-circuit current density (J_{SC}), maximum output voltage (P_{max}), voltage to get P_{max}, fill factor (FF), and power conversion efficiency (η) were investigated and analyzed for different parameters of the active layer and its thickness, and device series resistance. We compared all the simulation results for optimization of the power conversion efficiency of the OSCs.

Table 2 The default parameters of density of states of active layer P3HT:PCBM

Parameters	Symbol	Value
Electron trap density	–	4.207452×10^{24} m^{-3} eV^{-1}
Hole trap density	–	3.672318×10^{25} m^{-3} eV^{-1}
Electron tail slope	–	-100×10^{-3} eV
Hole tail slope	–	1.00×10^{-1} eV
Electron mobility	μ_e	5.00×10^{-9} $m^2V^{-1}s^1$
Hole mobility	μ_h	5.00×10^{-7} $m^2V^{-1}s^1$
Relative permittivity	ε_s	3 au
Number of traps	n	10 bands
Free electron to trapped electron	–	1.00×10^{-23} m^{-2}
Trapped electron to free hole	–	1.00×10^{-18} m^{-2}
Trapped hole to free electron	–	1.00×10^{-24} m^{-2}
Free hole to trapped hole	–	1.00×10^{-23} m^{-2}
Effective density of free electron states	N_e	5.00×10^{26} m^{-3}
Effective density of free hole states	N_h	5.00×10^{26} m^{-3}
–	X_i	3.7
Effective band gap	E_g	1.1 eV

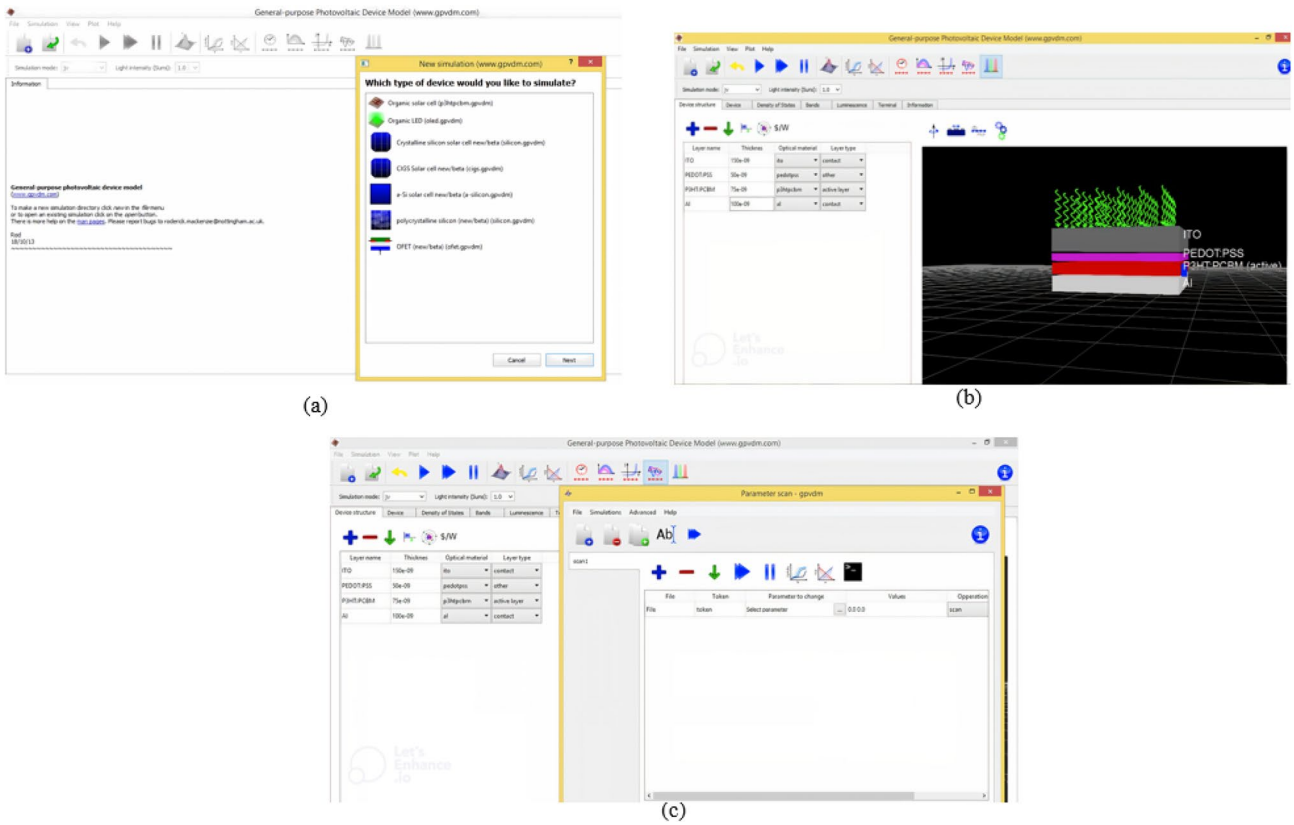

Fig. 2 GPVDM window: **a** opening window of simulator; **b** device structure after modeling the organic solar cell; **c** varying different parameters of different layers for the results comparison

J–V curve function of active layer for different density of states parameters

At first, we studied current density versus applied voltage (J–V) curves for different density of states of active layer (P3HT:PCBM) and optimized the value of the various density of states depending on the power conversion efficiency. We estimated the value of the most essential optical and electrical parameters of the organic solar cell, i.e., open-circuit voltage, short-circuit current density (J_{SC}), maximum output voltage, voltage to get P_{max}, fill factor, and power conversion efficiency.

Optimization of electron mobility

The performance characteristics of the ITO/PEDOT:PSS/P3HT:PCBM/Al-based heterojunction were measured as a function of electron mobility of active layer (P3HT:PCBM) under illumination. *J–V* characteristics were measured at 2.48×10^{-7} m^2V^{-1} s^{-1}, 2.48×10^{-8} m^2V^{-1} s^{-1}, 2.48×10^{-9} m^2V^{-1} s^{-1}, and 2.48×10^{-10} m^2V^{-1} s^{-1} to give a range of electron mobility. Figure 3 depicts a typical *J–V* curve of designed OSC for different electron mobility, and Table 3 summarizes V_{OC}, J_{SC},

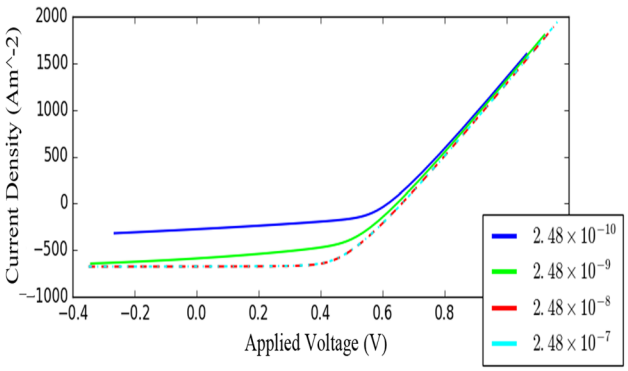

Fig. 3 *J–V* characteristics curve of the designed OSCs for different electron mobility (μ_e) of P3HT:PCBM: **a** $\mu_e=2.48\times10^{-7}$ m^2V^{-1} s^{-1} (dot sky blue line); **b** $\mu_e=2.48\times10^{-8}$ m^2V^{-1} s^{-1} (dash red line); **c** $\mu_e=2.48\times10^{-9}$ m^2V^{-1} s^{-1} (solid green line); and **d** $\mu_e=2.48\times10^{-10}$ m^2V^{-1} s^{-1} (solid blue line)

P_{max}, voltage to get P_{max}, *FF*, and η for different electron mobility. The device with electron mobility of 2.48×10^{-7} m^2V^{-1} s^{-1} showed a V_{OC} of 0.6624 V, J_{SC} of 675.44 Am^{-2}, *FF* of 59.63%, and η of 8.41%. After decreasing the electron mobility to 2.48×10^{-8} m^2V^{-1} s^{-1}, *VOC* decreased from 0.6624 to 0.6622 V, J_{SC} increased from

Table 3 The typical photovoltaic performance parameters of P3HT:PCBM with different electron mobility

Electron mobility; μ_e (m^2V^{-1} s^{-1})	Open-circuit voltage; V_{OC} (V)	Short-circuit current; J_{SC} (Am^{-2})	Maximum output power; P_{max} (Wm^{-2})	Voltage to get P_{max}; (V)	Fill factor; FF (%)	Power conversion efficiency; η (%)
2.48×10^{-7}	0.6624	675.44	266.81	0.4518	59.63	8.41
2.48×10^{-8}	0.6622	675.95	268.47	0.4505	59.97	8.47
2.48×10^{-9}	0.6464	590.99	198.54	0.4587	51.96	6.26
2.48×10^{-10}	0.6175	276.85	82.12	0.4700	48.03	2.59

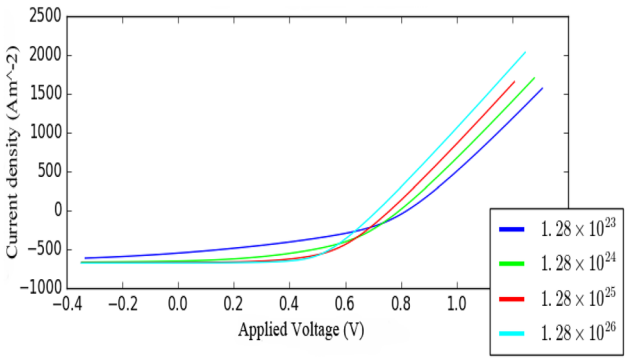

Fig. 4 *J–V* characteristics curve of the designed OSCs for different effective density of free electron states of P3HT:PCBM: **a** 1.28×10^{23} m^{-3} (solid blue line); **b** 1.28×10^{24} m^{-3} (solid green line); **c** 1.28×10^{25} m^{-3} (solid red line); and **d** 1.28×10^{26} m^{-3} (solid sky blue line)

675.44 to 675.95 Am^{-2}, and FF also increased, which in turn improved the PCE from 8.41 to 8.47%. Further decrease of electron mobility confirmed the decrease in the V_{OC}, J_{SC}, and FF, which in turn decreased the PCE of the organic solar cells.

PCE for electron mobility of 2.48×10^{-9} m^2V^{-1} s^{-1} and 2.48×10^{-10} m^2V^{-1} s^{-1} were 6.26% and 2.59%. Thus, electron mobility of 2.48×10^{-8} m^2V^{-1} s^{-1} is the optimum value of the active layer because we obtained maximum efficiency at this particular value. That's why, we considered electron mobility of 2.48×10^{-8} m^2V^{-1} s^{-1} for active layer throughout the research.

Optimization of effective density of free electron states

The performance characteristics of the ITO/PEDOT:PSS/P3HT:PCBM/Al-based heterojunction were measured as a function of effective density of free electron states of active layer, P3HT:PCBM under illumination. *J–V* characteristics were measured at 1.28×10^{23} m^{-3}, 1.28×10^{24} m^{-3}, 1.28×10^{25} m^{-3}, and 1.28×10^{26} m^{-3} to give a range of effective density of free electron states. Figure 4 depicts a typical *J–V* curve of designed OSC for different effective density of free electron states, and Table 4 summarizes V_{OC}, J_{SC}, P_{max}, voltage to get P_{max}, *FF*, and η for different effective density of free electron states.

From Fig. 4 and Table 4, it is obvious that the OSC device with 1.28×10^{23} m^{-3} as effective density of free electron states shows V_{OC} of 0.82 V, J_{SC} of 666.07 Am^{-2}, FF of 55.06%, and η of 9.50%. With increasing the value of effective density of free electron states, V_{OC} was decreasing and J_{SC} was increasing gradually. For an effective density of free electron states of 1.28×10^{24} m^{-3}, V_{OC} decreased from 0.82 to 0.7995 V, J_{SC} increased from 666.07 to 674.13 Am^{-2}, and FF increased from 55.06% to 61.56%. For this reason, PCE was also increased from 9.5 to 10.46%. Further increasing effective density of electron states 1.28×10^{25} m^{-3} showed V_{OC} of 0.7657 V, J_{SC} of 675.47 Am^{-2}, FF of 62.60% and power conversion efficiency of 10.21%. At this point, voltage decreasing is comparatively more than current density increasing.

Therefore, the maximum output power is lower than previous value of effective density of free electron states. At 1.28×10^{26} m^{-3}, though J_{SC} increased to 675.62 Am^{-2}, maximum output power as well as power conversion efficiency were decreased to 9.44% because V_{OC} and *FF* were

Table 4 The typical photovoltaic performance parameters of P3HT:PCBM with different effective density of free electron states

Effective density of free electron states; (m^{-3})	Open-circuit voltage; V_{OC} (V)	Short-circuit current; J_{SC} (Am^{-2})	Maximum output power; P_{max} (Wm^{-2})	Voltage to get P_{max}; (V)	Fill factor; FF (%)	Power conversion efficiency; η (%)
1.28×10^{23}	0.8200	666.07	301.02	0.5654	55.06	9.50
1.28×10^{24}	0.7995	674.13	331.83	0.5600	61.56	10.46
1.28×10^{25}	0.7657	675.47	323.82	0.5395	62.60	10.21
1.28×10^{26}	0.7183	675.62	299.26	0.4999	61.66	9.44

decreased to 0.7183 V and 61.66%. So 1.28×10^{24} m^{-3} effective density of free electron states is optimum value of the active layer (P3HT:PCBM) for high efficiency OSC, because we get maximum efficiency at this particular value in the simulation result. So, we fixed 2.48×10^{-8} m^2V^{-1} s^{-1} and 1.28×10^{24} m^{-3} as the value of electron mobility and effective density of free electron states for the active layer (P3HT:PCBM) density of states parameter taking PCE into consideration.

Optimization of effective density of free hole states

The performance characteristics of the ITO/PEDOT:PSS/P3HT:PCBM/Al-based heterojunction were measured as a function of effective density of free hole states of active layer, P3HT:PCBM under illumination. *J-V* characteristics were measured at 2.86×10^{22} m^{-3}, 2.86×10^{23} m^{-3}, 2.86×10^{24} m^{-3}, and 2.86×10^{25} m^{-3} to give a range of effective density of free hole states. Figure 5 depicts a typical *J–V* curve of designed OSC for different effective density of free hole states and Table 5 summarizes V_{OC}, J_{SC}, P_{max}, voltage to get P_{max}, *FF*, and η for different effective density of free hole states.

From Fig. 5 and Table 5, it is obvious that the OSC device with 2.86×10^{22} m^{-3} as effective density of free hole states showed V_{OC} of 1.06 V, J_{SC} of 574.46 Am^{-2}, FF of 60.37%, maximum output power of 368.25 Wm^{-2}, and PCE of 11.62%. By increasing the value of effective density of free hole states to 2.86×10^{23} m^{-3}, J–V curve produced V_{OC} of 0.9935 V, J_{SC} of 656.43 Am^{-2}, and FF of 60.09%. As V_{OC} was decreased, J_{SC} was increased but F*F* remained almost same, which in turn increased the PCE from 11.62 to 12.36%.

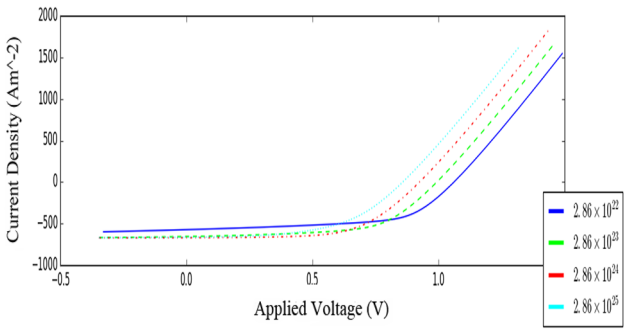

Fig. 5 *J–V* characteristics curve of the designed OSCs for different effective density of free hole states of P3HT:PCBM: **a** 2.86×10^{22} m^{-3} (solid blue line); **b** 2.86×10^{23} m^{-3} (dash green line); **c** 2.86×10^{24} m^{-3} (dash dot red line); and **d** 2.86×10^{25} m^{-3} (solid sky blue line)

Further rising the value of effective density of free hole states, V_{OC}, FF, as well as PCE have decreased; however, current density has increased. At 2.86×10^{24} m^{-3}, PCE was decreased to 11.74% and further increase of effective density of free hole states to2.86×10^{25} m^{-3} showed the power conversion efficiency of 9.63%. Therefore, 2.86×10^{23} m^{-3} as the effective density of free hole states is the optimum value of the active layer (P3HT:PCBM) for high efficiency OSC because we get maximum efficiency at this particular value in the simulation result. Thus, we fixed 2.48×10^{-8} m^2V^{-1} s^{-1}, 1.28×10^{24} m^{-3}, and 2.86×10^{23} m^{-3} as the optimized value of electron mobility, effective density of free electron states, and effective density of free hole states for the active layer (P3HT:PCBM) density of states parameter taking PCE into consideration.

Optimization of hole mobility

The performance characteristics of the ITO/PEDOT:PSS/P3HT:PCBM/Al-based heterojunction were measured as a function of hole mobility of active layer (P3HT:PCBM) under illumination. *J–V* characteristics were measured at 2.48×10^{-6} m^2V^{-1} $s^{-}1$, 2.48×10^{-7} m^2V^{-1} s^{-1}, 2.48×10^{-8} m^2V^{-1} s^{-1}, and 2.48×10^{-9} m^2V^{-1} s^{-1} to give a wide range of hole mobility. Figure 6 shows a typical *J–V* curve of designed OSC for different hole mobility and Table 6 summarizes V_{OC}, J_{SC}, P_{max}, voltage to get P_{max}, *FF*, and η for different hole mobility.

From Fig. 6 and Table 6, it is evident that current density (J_{SC}) and power conversion efficiency showed decreasing trend with the decrease of hole mobility. We achieved the maximum PCE at a hole mobility of 2.48×10^{-6} m^2V^{-1} s^{-1}. Therefore, we achieved the optimum value of hole mobility at a value of 2.48×10^{-6} m^2V^{-1} s^{-1} of the active layer for high efficiency OSC, because we achieved maximum efficiency at this particular value in the simulation result. Thus,

Table 5 The typical photovoltaic performance parameters of P3HT:PCBM with different effective density of free hole states

Effective density of free hole states; (m^{-3})	Open-circuit voltage; V_{OC} (V)	Short-circuit current; J_{SC} (Am^{-2})	Maximum output power; P_{max} (Wm^{-2})	Voltage to get P_{max}; (V)	Fill factor; FF (%)	Power conversion efficiency η (%)
2.86×10^{22}	1.0600	574.46	368.25	0.8256	60.37	11.62
2.86×10^{23}	0.9935	656.43	391.97	0.7352	60.09	12.36
2.86×10^{24}	0.9248	670.40	372.14	0.6449	60.02	11.74
2.86×10^{25}	0.8585	664.49	305.35	0.5886	53.52	9.63

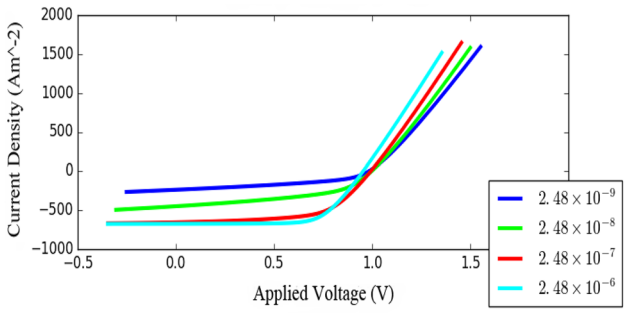

Fig. 6 *J–V* characteristics curve of the designed OSCs for different hole mobility (μ_h) of P3HT:PCBM: **a** $\mu_h = 2.48 \times 10^{-9}$ m^2V^{-1} s^{-1} (solid blue line); **b** $\mu_h = 2.48 \times 10^{-8}$ m^2V^{-1} s^{-1} (solid green line); **c** $\mu_h = 2.48 \times 10^{-7}$ m^2V^{-1} s^{-1} (solid red line); and **d** $\mu_h = 2.48 \times 10^{-6}$ m^2V^{-1} s^{-1} (solid sky blue line)

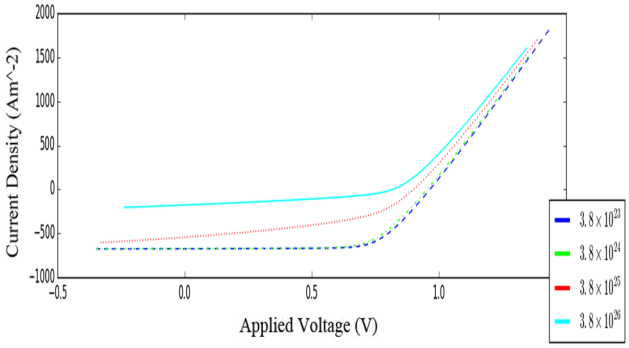

Fig. 7 *J–V* characteristics curve of the designed OSCs for different electron trap density of P3HT:PCBM: **a** 3.8×10^{23} m^3eV^{-1} (dash blue line); **b** 3.8×10^{24} m^3eV^{-1} (das dot green line); **c** 3.8×10^{25} m^3eV^{-1} (dot red line); and **d** 3.8×10^{26} m^3eV^{-1} (solid sky blue line)

we fixed 2.48×10^{-6} m^2V^{-1} s^{-1}, 2.48×10^{-8} m^2V^{-1} s^{-1}, 1.28×10^{24} m^{-3}, and 2.86×10^{23} m^{-3} as the optimized value of hole mobility, electron mobility, and effective density of free electron states and effective density of free hole states for the active layer (P3HT:PCBM) density of states parameter taking the PCE into consideration.

Optimization of electron trap density

The performance characteristics of the ITO/PEDOT:PSS/P3HT:PCBM/Al-based heterojunction were determined as a function of electron trap density of active layer (P3HT:PCBM) under illumination. *J–V* characteristics were simulated at 3.8×10^{23} m^3eV^{-1}, 3.8×10^{24} m^3eV^{-1}, 3.8×10^{25} m^3eV^{-1}, and 3.8×10^{26} m^3eV^{-1} to give a range of electron trap density. Figure 7 represents a typical *J–V* curve of designed OSC for different electron trap density, and Table 7 summarizes V_{OC}, J_{SC}, P_{max}, voltage to get P_{max}, *FF*, and η for different electron trap density. From Fig. 7 and Table 7, it is obvious that current density (J_{SC}) and power conversion efficiency decreased rapidly with the increasing of electron trap density.

Therefore, we achieved the optimum value of electron trap density at a value of 3.8×10^{23} m^3eV^{-1} of active layer for high-efficiency OSC, because we achieved maximum efficiency (14.17%) at this particular value in the simulation result. Thus, we fixed 3.8×10^{23} m^3eV^{-1}, 2.48×10^{-6} m^2V^{-1} s^{-1}, 2.48×10^{-8} m^2V^{-1} s^{-1}, 1.28×10^{24} m^{-3}, and 2.86×10^{23} m^{-3} as the optimized value of electron trap density, hole mobility, electron mobility, effective density of free electron states, and effective density of free hole states for the active layer (P3HT:PCBM) density of states parameter taking the PCE into consideration.

Optimization of hole trap density

The performance characteristics of the ITO/PEDOT:PSS/P3HT:PCBM/Al-based heterojunction were determined as a function of hole trap density of active layer (P3HT:PCBM) under illumination. *J-V* characteristics were simulated at 1.45×10^{23} m^3eV^{-1}, 1.45×10^{24} m^3eV^{-1}, 1.45×10^{25} m^3eV^{-1}, and 1.45×10^{26} m^3eV^{-1} to give a range of hole trap density. Figure 8 shows a typical *J–V* curve of designed OSC for different hole trap density, and Table 8 summarizes V_{OC}, J_{SC}, P_{max}, voltage to get P_{max}, *FF*, and η for different hole trap density. At a hole trap density of 1.45×10^{23} m^3eV^{-1}, OSC device produced V_{OC} of 0.9581 V, J_{SC} of 676.70 Am^{-2}, FF of 71.22%, and η of 14.54%. With increasing the hole trap density to 1.45×10^{24} m^3eV^{-1}, V_{OC} increased from 0.9581 to 0.9593 V, J_{SC} increased from 676.70 to 676.74 Am^{-2}, and FF increased from 71.22 to 71.47%, which in turn increased the η from 14.54 to 14.61%. Further, increasing the value of

Table 6 The typical photovoltaic performance parameters of P3HT:PCBM with different hole mobility

Hole mobility; μ_h (m^2V^{-1} s^{-1})	Open-circuit voltage; V_{OC} (V)	Short-circuit current; J_{SC} (Am^{-2})	Maximum output power; P_{max} (Wm^{-2})	Voltage to get P_{max}; (V)	Fill factor; FF (%)	Power conversion efficiency η (%)
2.48×10^{-6}	0.9500	674.44	433.56	0.7063	67.38	13.67
2.48×10^{-7}	0.9900	656.42	391.96	0.7352	60.09	12.36
2.48×10^{-8}	0.9977	450.67	215.00	0.7532	47.81	6.78
2.48×10^{-9}	0.9996	317.85	143.60	0.5700	45.03	4.53

Table 7 The typical photovoltaic performance parameters of P3HT:PCBM with different electron trap density

Electron trap density; (m^3eV^{-1})	Open-circuit voltage; V_{OC} (V)	Short-circuit current; J_{SC} (Am^{-2})	Maximum output power; P_{max} (Wm^{-2})	Voltage to get P_{max}; (V)	Fill factor; FF (%)	Power conversion efficiency η (%)
3.8×10^{23}	0.9651	675.59	449.81	0.7247	68.98	14.17
3.8×10^{24}	0.9539	674.44	433.56	0.7063	67.35	13.66
3.8×10^{25}	0.9011	546.49	222.63	0.6498	45.20	7.01
3.8×10^{26}	0.8193	178.96	55.34	0.5567	37.74	1.74

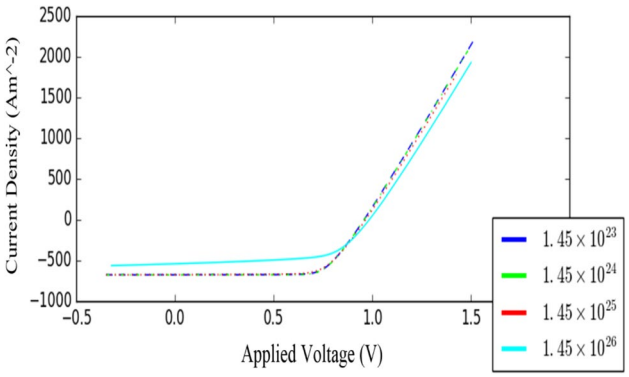

Fig. 8 *J–V* characteristics curve of the designed OSCs for different hole trap density of P3HT:PCBM: **a** 1.45×10^{23} m^3eV^{-1} (dash blue line); **b** 1.45×10^{24} m^3eV^{-1} (das dot green line); **c** 1.45×10^{25} m^3eV^{-1} (dot red line); and **d** 1.45×10^{26} m^3eV^{-1} (solid sky blue line)

hole trap density to 1.45×10^{25} m^3eV^{-1}, V_{OC} increased to 0.9665 but J_{SC} decreased to 675.64 Am^{-2} and FF decreased to 69.09%, which in turn decreased the η to 14.21%.

From Fig. 8 and Table 8, it is evident that for further increasing in hole trap density, V_{OC} increased slowly but J_{SC}, FF decreased rapidly, which in turn decreased the value of η. Therefore, we achieved the optimum value of hole trap density at a value of 1.45×10^{24} m^3eV^{-1} of the active layer for high efficiency OSC, because we achieved maximum efficiency (14.61%) at this particular value in the simulation result. Thus, we fixed 1.45×10^{24} m^3eV^{-1}, 3.8×10^{23} m^3eV^{-1}, 2.48×10^{-6} m^2V^{-1} s^{-1}, 2.48×10^{-8} m^2V^{-1} s^{-1}, 1.28×10^{24} m^{-3}, and 2.86×10^{23} m^{-3} as the optimized value of hole trap density, electron trap density, hole mobility, electron mobility, effective density of free electron states, and effective density of free hole states for the active layer (P3HT:PCBM) density of states parameter taking the PCE into consideration. The above value is the optimum value of different density of states parameters of active layer which produced the maximum PCE for our designed OSCs.

Optimization of active layer thickness

The performance of the thickness of the active layer (P3HT:PCBM) was investigated for the ITO/PEDOT:PSS/P3HT:PCBM/Al-based bulk heterojunction organic solar cell under illumination. We varied the thickness of the active layer from 50 to 225 nm to optimize the thickness value for designing higher OSCs. *J–V* characteristics were simulated at 50 nm, 75 nm, 100 nm, and 125 nm as shown in Fig. 9 as well as 150 nm, 175 nm, 200 nm, and 225 nm as shown in Fig. 10 to give a wide range of active layer thickness. Therefore, Figs. 9 and 10 depict typical *J–V* curve of designed OSC for different active layer thickness and Table 9 summarizes V_{OC}, J_{SC}, P_{max}, voltage to get P_{max}, *FF,* and η for different active layer thickness. From Fig. 9 and Table 9, it is evident that the device with a thickness of 50 nm produces V_{OC} of 0.9516 V, J_{SC} of 652.84 Am^{-2}, FF of 71.98%, and η of 14.08%.

Since the free carriers generated in a thicker active layer could not be efficiently collected by the electrodes, the lower current was obtained. But the V_{OC} of the solar cells seems to be independent of the active film thickness; all of them had a V_{OC} about 0.96 V. With increase thickness to 75 nm, V_{OC} increased from 0.9516 to 0.9584 V, J_{SC} increased to highest value of 735.87 Am^{-2} and FF decreased from 71.98 to 70.32%. As V_{OC} and FF change is very small and J_{SC} is highest, so the PCE increased

Table 8 The typical photovoltaic performance parameters of P3HT:PCBM with different hole trap density

Hole trap density; (m^3eV^{-1})	Open-circuit voltage; V_{OC} (V)	Short-circuit current; J_{SC} (Am^{-2})	Maximum output power; P_{max} (Wm^{-2})	Voltage to get P_{max}; (V)	Fill factor; FF (%)	Power conversion efficiency; η (%)
1.45×10^{23}	0.9581	676.70	461.84	0.7198	71.22	14.54
1.45×10^{24}	0.9593	676.74	464.04	0.7189	71.47	14.61
1.45×10^{25}	0.9665	675.64	451.23	0.7241	69.09	14.21
1.45×10^{26}	0.9846	541.25	333.24	0.7569	62.52	10.50

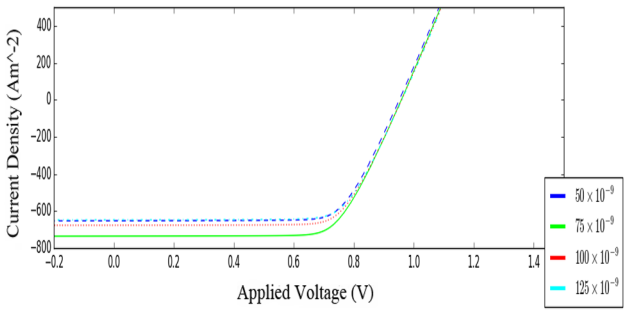

Fig. 9 *J–V* characteristics curve of the designed OSCs for different thickness (*d*) of active layer: **a** *d* = 50 nm (dash blue line); **b** *d* = 75 nm (solid green line); **c** *d* = 100 nm (dot red line); and **d** *d* = 125 nm (dash dot sky blue line)

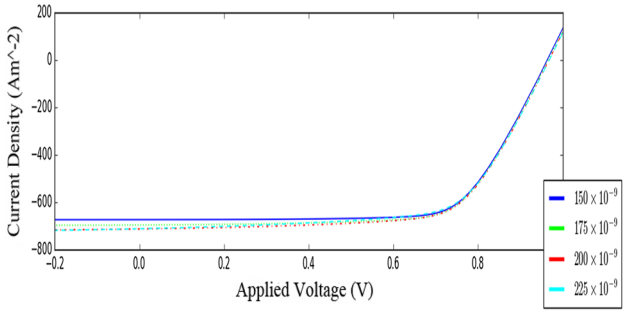

Fig. 10 *J–V* characteristics curve of the designed OSCs for different thickness (*d*) of active layer: **a** *d* = 150 nm (solid blue line); **b** *d* = 175 nm (dot green line); **c** *d* = 200 nm (dash dot red line); and **d** *d* = 225 nm (dash sky blue line)

from 14.08 to 15.62%. Further increase of layer thickness, V_{OC} increased slowly but J_{SC} decreased till the thickness reached down to 125 nm and started increasing again. The FF also decreased with increasing thickness. Thus, PCE of OSC decreased up to 125 nm thickness of the active layer. Though current density, J_{SC} increased with thickness more than 125 nm, maximum output power could not exceed at the active layer thickness value of 75 nm (495.96 Am^{-2}) because with increasing layer thickness more than 125 nm, FF decreased, which in turn decreased the PCE. That's why we considered 75 nm as the optimum value of thickness of the active layer. We achieved maximum efficiency at this particular value.

Optimization of device series resistance

The performance of the device series resistance of the ITO/PEDOT:PSS/P3HT:PCBM/Al-based bulk heterojunction organic solar cells was evaluated under illumination. We varied the device series resistance from 15 to 30 Ω to optimize the resistances for designing higher OSCs. The illumination *J-V* characteristics were simulated at different device series resistances, i.e., 15 Ω, 20 Ω, 25 Ω, and 30 Ω. Figure 11 illustrates a typical *J–V* curve of designed OSC for different series resistance, and Table 10 summarizes V_{OC}, J_{SC}, P_{max}, voltage to get P_{max}, FF, and η for different series resistance.

From Fig. 11 and Table 10, it is obvious that the J_{SC} and FF changed with the increase in resistance, J_{SC} reached maximum at 15 Ω and minimum at 30 Ω. At 15 Ω resistance, J_{SC} and *FF* had the highest value, which in turn produced highest value of PCE (16.46%). With increasing resistances, J_{SC} and FF decreased, which in turn decreased the value of PCE. Thus, low device series resistance gives maximum power conversion efficiency for OSCs. The value of PCE was inversely proportional to the series resistance. In addition, fill factor was also inversely proportional with the series resistance. Accordingly, a device series resistance of 15 Ω was considered as the optimum value because we obtained maximum power conversion efficiency at this particular value. The active area makes the photo-generated current travel a longer distance before it is collected at the electrodes. In this work, a thick grid was applied to maintain a low effective resistance of the ITO.

Table 9 The typical photovoltaic performance parameters with different active layer thickness

Active layer thickness; *d* (nm)	Open-circuit voltage; V_{OC} (V)	Short-circuit current; J_{SC} (Am^{-2})	Maximum output power; P_{max} (Wm^{-2})	Voltage to get P_{max}; (V)	Fill factor; FF (%)	Power conversion efficiency η (%)
50	0.9516	652.84	447.25	0.7258	71.98	14.08
75	0.9584	735.87	495.96	0.7184	70.32	15.62
100	0.9593	676.74	464.04	0.7189	71.47	14.62
125	0.9600	647.90	446.80	0.7250	71.78	14.07
150	0.9634	675.41	458.47	0.7330	70.46	14.44
175	0.9665	714.64	471.00	0.7280	68.18	14.83
200	0.9674	713.25	463.14	0.7310	67.11	14.59
225	0.9687	723.17	461.19	0.7320	65.83	14.52

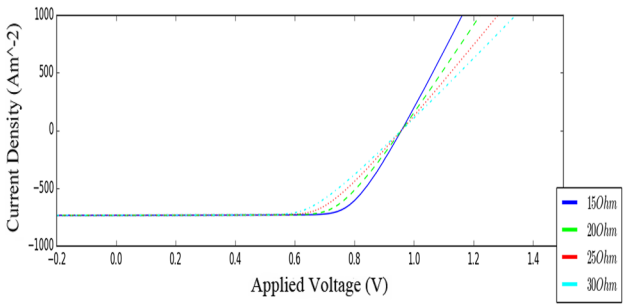

Fig. 11 *J–V* characteristics curve of the designed OSCs for different device series resistance (*R*): **a** $R=15$ Ohm (solid blue line); **b** $R=20$ Ohm (dash green line); **c** $R=25$ Ohm (dot red line); and **d** $R=30$ Ohm (dash dot sky blue line)

Overall power conversion efficiency (PCE) of designed OSCs

We selected the optimize value of different parameters of active layer (P3HT:PCBM), active layer thickness, and device series resistance to get higher efficiency of OSCs. We selected the value of 2.48×10^{-8} m^2v^{-1} s^{-1} for electron mobility, 2.48×10^{-6} m^2v^{-1} s^{-1} for hole mobility, 1.28×10^{24} m^{-3} for effective density of free electron states, 2.86×10^{23} m^{-3} for effective density of free hole states, 3.8×10^{23} m^3eV^{-1} for electron trap density, and 1.45×10^{24} m^3eV^{-1} for hole trap density using efficiency calculation from *J* to *V* curve. Furthermore, we selected the active layer thickness and device series resistance value as 75 nm and 15 Ω to achieve maximum power conversion efficiency. After considering the optimized value of different parameters of designed OSCs, we achieved a maximum power conversion efficiency of 16.46% and a maximum fill factor of 74.09%.

Conclusion

Solar energy is considered as the energy of the future as it is renewable and has small impact on the environment. We designed high efficient bulk heterojunction organic solar cell by selecting appropriate materials. We optimized the active layer materials' properties such as electron mobility, hole mobility, effective density of free electron states, effective density of free hole states, electron trap density, hole trap density, and electrical properties such as device series resistance, thickness of the active layer depending on the maximum power conversion efficiency of the designed OSCs. Maximum power conversion efficiency of 16.46% was achieved for the lowest device series resistance of 15 Ω. Thus, lower value of device series resistance gives maximum power conversion efficiency compared to the higher value of device series resistance for OSCs. In addition, an optimized value of 75 nm was obtained as an active layer thickness for the designed OSCs depending on the maximum value of the PCE. We strongly believe that adequate research in this field will provide us OSCs having good optical and electrical properties. In addition, the designed OSCs can be fabricated in future using the widely used fabrication technique for commercialization.

Table 10 The typical photovoltaic performance parameters of different device series resistance

Series resistance; *R* (Ohm)	Open-circuit voltage; V_{OC} (V)	Short-circuit current; J_{SC} (Am^{-2})	Maximum output power; P_{max} (Wm^{-2})	Voltage to get P_{max}; (V)	Fill factor; FF (%)	Power conversion efficiency η (%)
15	0.9584	735.97	522.64	0.7434	74.09	16.46
20	0.9584	735.87	493.10	0.7143	69.91	15.53
25	0.9584	735.75	464.51	0.6729	65.87	14.63
30	0.9584	735.65	435.92	0.6314	61.82	13.73

Funding No funding was received to assist with the preparation of this manuscript.

Data availability The data supporting the findings of this study and its supplementary materials are available within the manuscript.

Declarations

Conflict of interest The authors have no conflicts of interest to disclose.

References

1. A. Toor, Renewables projected to overtake natural gas as world's second largest power source (2013), http://www.theverge.com/2013/6/28/44773694/. Accessed 25 Nov 2022
2. M. Lenes, Efficiency Enhancement of Polymer Fullerene Solar Cells. Ph.D thesis, (Zernike Institute, Univ. of Groningen, The Netherlands, 2009–13).
3. M. Pagliaro, G. Palmisano, R. Ciriminna, *Flexible Solar Cells*, Chap. 1, (Institute for Nanostructured Materials, Palermo, Italy, 2008), p. 3–4
4. G. Li, V. Shrotriya, J. Huang, Y. Yao, T. Moriarty, K. Emeryand, Y. Yang, High-efficiency solution processable polymer photovoltaic cells by self-organization of polymer blends. Nat. Mater. **4**, 864–868 (2005)
5. C.J. Brabec, N.S. Sariciftci, J.C. Hummelen, Plastic solar cells. Adv. Func. Mater. **11**, 15–26 (2011)
6. V.E. Ferry, J.N. Munday, H.A. Atwater, Design considerations for plasmonic photovoltaics. Adv. Mater. **22**, 4794–4808 (2010)
7. J. Barker, C. Ramsdale, N. Greenham, Modeling the current-voltage characteristics of bilayer polymer photovoltaic devices. Phys. Rev. B **67**, 1–9 (2003)
8. G. Buxton, N. Clarke, Predicting structure and property relations in polymeric photovoltaic devices. Phys. Rev. B **74**, 1–5 (2006)
9. C.M. Martin, V.M. Burlakov, H.E. Assender, D.A.R. Barkhouse, A numerical model for explaining the role of the interface morphology in composite solar cells. Appl. Phys. **102**, 104–506 (2007)
10. J. Williams, A.B. Walker, Two-dimensional simulations of bulk heterojunction solar cell characteristics. Nanotechnology **19**, 424011 (2008)
11. M. Shah, V. Ganesan, Correlations between morphologies and photovoltaic properties of RodCoil block copolymers. Macromolecules **43**, 543–552 (2010)
12. A. Abulimuand, D. Barbero, *Measuring the Efficiency and Charge Carrier Mobility of Organic Solar Cells*, (Depart. of Physics, Umeå Univ., Sweden, 2012)
13. Y. Yuan, T.J. Reece, P. Sharma, S. Poddar, S. Ducharme, Efficiency enhancement in organic solar cells with ferroelectric polymers. Nat. Mater. **10**, 296–302 (2011)
14. P. Hudhomme, An overview of molecular acceptors for organic solar cells. Photovolt. **4**, 40401 (2013)
15. J.-S. Yeo, J.-M. Yun, S.-S. Kim, D.-Y. Kim, J. Kim, S.-I. Na, Variations of cell performance in ITO-free organic solar cells with increasing cell areas. Semicond. Sci. Technol. **26**, 034010 (2011)
16. P. Peumans, V. Bulovic, S.R. Forest, Efficient photon harvesting at high optical and electrical intensities in ultrathin organic double-heterostructure photovoltaic diodes. Appl. Phys. Lett. **76**, 26–50 (2000)
17. M. Niggemann, M. Glatthaar, P. Lewer, C. Muller, J. Wagner, A. Gombert, Trapping light with micro lenses in thin film organic photovoltaic cells. Thin Solid Films **511**, 628–633 (2006)
18. S. Rim, S. Zhao, S.R. Scully, M.D. McGehee, P. Peumans, An effective light trapping configuration for thin-film solar cells. Appl. Phys. Lett. **91**, 501 (2007)
19. C.Y. Liu, Hybrid solar cells from polymers and silicon nanocrystals. ASME 3rd International conference on energy sustainability 1, 985–987 (2009)
20. H. Ade, New materials yield record efficiency polymer solar cells. (2014), http://www.konarka.com/index.php/site/. Accessed 25 Nov 2022
21. F.C. Krebs, *Polymeric Solar Cells Materials Design Manufacture* (DEStech Publications Inc., Lancaster, 2010)
22. Solid States Technology, Organic Electronics Workshop. (2011) http://www.electroiq.com/articles/sst/2011/. Accessed 25 Nov 2022
23. Lisa Zyga, Solar cell sets world record with a stabilized efficiency of 13.6%. http://phys.org/news/2015-06. Accessed 25 Nov 2022
24. Abu Kowsar et al., Comparative study on solar cell simulators. International Conference on innovation in engineering and technology (ICIET), (2019)
25. R.B. Kodati et al., A review of solar cell fundamentals and technologies. Adv. Sci. Lett. **26**(5), 260–271 (2020)
26. R.B. Kodati et al., A survey of solar cell. Adv. Sci. Lett. **26**(5), 1060–1065 (2020)
27. R. Rabeya et al. Design and performance analysis of multijunction organic solar cell exceeding 14% efficiency. 2018 10th International conference on electrical and computer engineering (ICECE), 321–324 (2018)
28. J. Singh et al., Optimizing the design of flexible PTB7:PC71BM bulk heterojunction and P3HT:SiNW hybrid organic solar cells. Nanosci. Technol. (2014). https://doi.org/10.15226/2374-8141/1/1/00103
29. Y. Ogata et al., Paper dye-sensitized solar cell based on carbon-nanotube-composite papers. Energies **13**, 57 (2020)
30. P. Meredith et al., Scaling of next generation solution processed organic and perovskite solar cells. Nat. Commun. (2018). https://doi.org/10.1038/s41467-018-05514-9
31. R. Zhou et al., All-small-molecule organic solar cells with over 14% efficiency by optimizing hierarchical morphologies. Nat. Commun. (2019). https://doi.org/10.1038/s41467-019-13292-1
32. M. Farrokhifar, A. Rostami, N. Sadoogi, Opto-electrical simulation of organic solar cells. UKSim-AMSS 8th European modelling symposium, Pisa Pisa, Italy, (2014)
33. S. Oh, D. Yeo, K. Park, H. Kim, Performance enhancement of organic solar cells with the LiF/Al cathode structure by the pyromellitic dianhydride layer. Adv. Mater. Res. **415–417**, 1608–1610 (2012)
34. N. Rastogi, N. Singh, Electrical simulation of organic solar cell at different series resistances and different temperatures. IOSR J. Appl. Phys. **8**, 54–57 (2016)
35. M. Polyanskiy, Refractive index database. https://refractiveindex.info. Accessed 25 Nov 2022